Progress In Electromagnetics Research, Vol. 106, 243–261, 2010

MODAL METHOD BASED ON SPLINE EXPANSION FOR THE ELECTROMAGNETIC ANALYSIS OF THE LAMELLAR GRATING

A. M. Armeanu †

Laboratoire des Technologies de la Microélectronique CNRS
17 rue des Martyrs, F-38054 Grenoble Cedex 09, France

K. Edee and G. Granet ‡

CNRS
UMR 6602, LASMEA, F-63177 Aubière, France

P. Schiavone §

Laboratoire des Technologies de la Microélectronique CNRS
17 rue des Martyrs, F-38054 Grenoble Cedex 09, France

Abstract—This paper reports an exact and explicit representation of the differential operators from Maxwell's equations. In order to solve these equations, the spline basis functions with compact support are used. We describe the electromagnetic analysis of the lamellar grating as an eigenvalues problem. We choose the second degree spline as basis functions. The basis functions are projected onto a set of test functions. We use and compare several test functions namely: Dirac, Pulse and Spline. We show that the choice of the basis and test functions has a great influence on the convergence speed. The outcomes are compared with those obtained by implementing the Finite-Difference Modal Method which is used as a reference. In order to improve the numerical results an adaptive spatial resolution is used. Compared to the reference method, we show a significantly improved convergence when using the spline expansion projected onto spline test functions.

Received 19 February 2010, Accepted 1 April 2010, Scheduled 25 July 2010
Corresponding author: A. M. Armeanu (ana-maria.armeanu@cea.fr).
† Also with CNRS, UMR 6602, LASMEA, F-63177 Aubière, France.
‡ K. Edee and G. Granet are also with Clermont Universités, Université Blaise Pascal, LASMEA, BP10448, F-63000 Clermont-Ferrand, France.
§ Also with UMI2958 CNRS-Georgia Tech., Georgia Institute of Technology, 777 Atlantic Dr, Atlanta, GA 30332, USA.

1. INTRODUCTION

Modal methods and mode matching techniques are well established methods to solve wave guide and scattering problems. One of their interesting features is that they easily allow understanding and giving some physical insight into the physical phenomena. For lamellar gratings, the eigenfunctions of the Helmoltz equation can be written in an analytical form in which the only numerical parameters — the eigenvalues-are obtained as the zeros of a transcendental equation [1, 2]. However in the case of materials with complex permittivity, determining the roots of the transcendental eigenvalue equation requires quite sophisticated mathematics in order to overcome numerical difficulties. In practice, numerical methods are indispensable in the analysis of gratings and related devices. The Fourier Modal Method [3] or the differential method [4] are well spread methods in this field. They share a common feature: in both of them the field is expanded into a Fourier basis. This choice is known to lead to slow convergence in the case of large index contrast or when the index profile variation is very localized. Subwavelength slits arrays in metallic films are typical examples of such a situation. Hence, one can wonder if other expansions would be more efficient. Within the framework of modal methods, The Finite Difference Modal Method [6] is one such attempt. It can be considered as a modal method in which the field is expanded into pulse functions. On the other hand, multiresolution strategies have been proposed and the application of wavelets in computational electromagnetics or quantum mechanics [7] has attracted a great deal of attention [8]. In most of these papers, wavelets are used as an efficient way for matrix compression [9]. Many inverse problems have been analyzed by using wavelets as well. However, to the best of our knowledge, they have not been introduced in the formulation of eigenvalue problems in electromagnetism.

This paper is a preliminary work in this direction. It is devoted to the modal analysis of one dimensional lamellar gratings using spline basis as was suggested by Edee et al. [10, 11]. The latter basis have the valuable property of being continuous as well as compact support functions.

The modal method based on spline expansion is described in Section 2. In Section 3, the convergence speed is studied for the metal and dielectric gratings for the TE and TM polarizations. It is compared with the one achieved with the non uniform version of the Finite Difference Modal Method reported in [6]. Section 3 concludes the paper.

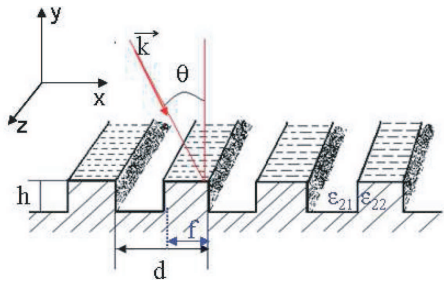

Figure 1. Schematic of the classical grating diffraction problem.

2. MODAL METHOD BASED ON SPLINE EXPANSION

2.1. Description of the Problem

Let us consider the canonical case of the one dimensional lamellar grating in the case of the so-called classical incidence [12] illustrated in Figure 1. This structure is invariant along the z direction and is illuminated by a monochromatic plane wave that can be either TE (the only non-null components of the fields are H_x, H_y, E_z) or TM (the only non-null components of the fields are E_x, E_y, H_z) polarized. We denote λ the wavelength of the incident wave, $\mathbf{k}$ its wave vector and ω the angular frequency. The direction of the wave vector is given by the angle $\theta = (\mathbf{k}, \mathbf{Oy})$. The time dependence expressed by the term $\exp(i\omega t)$ is omitted in the rest of this publication. It is well known that in these cases of polarization the electromagnetic field can be expressed in terms of E_z and H_z for the TE and TM polarization case respectively [12]. Taking into account that the permittivity of the inhomogeneous medium, $\varepsilon(x)$, depends only on the x variable, each component of the electromagnetic field can be expressed as the product of two functions of a single variable in the form of:

$$\Phi(x, y) = f(x)e^{-ikry}$$

where $k = 2\pi/\lambda$ is the wave number.

Hence, Maxwell's equations can be written as:

$$\text{TE}: \begin{cases} -ikrE_z(x) = -i\omega\mu_0 H_x(x) \\ \partial_x E_z(x) = i\omega\mu_0 H_y(x) \\ \partial_x H_y(x) + ikrH_x(x) = i\omega\varepsilon_0\varepsilon(x)E_z(x), \end{cases} \tag{1}$$

$$\text{TM}: \begin{cases} \dfrac{-ikr}{\varepsilon_0}\dfrac{1}{\varepsilon(x)}H_z(x) = i\omega\ E_x(x) \\ \partial_x H_z(x) = -i\omega\varepsilon_0\varepsilon(x)E_y(x) \\ \partial_x E_y(x) + ikrE_x(x) = -i\omega\mu_0 H_z(x), \end{cases} \tag{2}$$

where the constant μ_0 and ε_0 denote the vacuum permeability and permittivity. The unidimensional grating is placed between two homogeneous regions (the superstrate and the substrate) and is characterized by a periodic permittivity $\varepsilon_2(x)$ with a period d.

$$\varepsilon_2(x) = \begin{cases} \varepsilon_{21} & \text{for} \quad 0 \le x \le fd \\ \varepsilon_{22} & \text{for} \quad fd \le x \le d, \end{cases} \tag{3}$$

where f is the fill factor.

Our aim is to numerically solve the lamellar grating diffraction problem. For that purpose, the method of moments is used.

2.2. Method of Moments: Uniform Sampling Scheme

We apply the method of moments [13] for the computation of the electromagnetic field [14]. All the components of the electromagnetic field are expanded into a sum of basis functions B_n. The x varying part of each component of the field is expressed as:

$$f(x) = \sum_{n=1}^{\infty} f_n B_n(x). \tag{4}$$

By projecting the Equations (1) and (2) onto a set of test functions T_q for both polarizations we obtain:

$$\begin{cases} -ikr \left\langle T_q(x), \sum_n E_{z_n} B_n(x) \right\rangle = -i\omega\mu_0 \left\langle T_q(x), \sum_n H_{x_n} B_n(x) \right\rangle \\ \left\langle T_q(x), \sum_n E_{z_n} \dfrac{d}{dx} B_n(x) \right\rangle = i\omega\mu_0 \left\langle T_q(x), \sum_n H_{y_n} B_n(x) \right\rangle \\ \left\langle T_q(x), \sum_n H_{y_n} \dfrac{d}{dx} B_n(x) \right\rangle + ikr \left\langle T_q(x), \sum_n H_{x_n} B_n(x) \right\rangle \\ \qquad = i\omega\varepsilon_0 \left\langle T_q(x), \sum_n \varepsilon(x) E_{z_n} B_n(x) \right\rangle \end{cases} \tag{5}$$

for the TE polarization.

$$\begin{cases} \dfrac{-ikr}{\varepsilon_0} \left\langle T_q(x), \sum_n \dfrac{1}{\varepsilon(x)} H_{z_n} B_n(x) \right\rangle = i\omega \left\langle T_q(x), \sum_n E_{x_n} B_n(x) \right\rangle \\ \left\langle T_q(x), \sum_n H_{z_n} \dfrac{d}{dx} B_n(x) \right\rangle = -i\omega\varepsilon_0 \left\langle T_q(x), \sum_n \varepsilon(x) E_{y_n} B_n(x) \right\rangle \\ \left\langle T_q(x), \sum_n E_{y_n} \dfrac{d}{dx} B_n(x) \right\rangle + ikr \left\langle T_q(x), \sum_n E_{x_n} B_n(x) \right\rangle \\ = -i\omega\mu_0 \left\langle T_q(x), \sum_n E_{z_n} B_n(x) \right\rangle \end{cases} \tag{6}$$

for the TM polarization.

$\langle u, v \rangle$ denotes the hermitian inner product of two functions u and v. When we numerically implement the above equations, we only

take into account a finite set of basis functions, so only N terms are considered.

The first step in applying this method is to select a discrete set of points along x direction. These points are denoted as $x_n = nd/N$ with $n \in \{-2, -1, \ldots, N+2\}$. On the interval $d/N\,[-2, N+2]$ we define B_n^N, a set of basis functions. The B_n^N are modified in order to take into account the pseudoperiodicity of the electromagnetic field:

$$B_n^N(x) = e^{(-ik\alpha_0 x)}\tilde{B}_n^N(x) \qquad \text{with } \alpha_0 = \sin(\theta)$$

where $\tilde{B}_n^N$ is a quadratic spline function (see Figure 2) defined as:

$$\tilde{B}_n^N(x) = \frac{3}{N}\begin{cases} \dfrac{1}{2}\left(x - \dfrac{nd}{N}\right)^2 & x \in \dfrac{d}{N}[n, n+1] \\ -\left(x - \dfrac{d}{N}\left(n + \dfrac{3}{2}\right)\right)^2 + \dfrac{3}{4}\left(\dfrac{d}{N}\right)^2 & x \in \dfrac{d}{N}[n+1, n+2] \\ \dfrac{1}{2}\left(x^2 - \dfrac{d}{N}(n+3)\right)^2 & x \in \dfrac{d}{N}[n+2, n+3] \\ 0 & \text{otherwise} \end{cases} \tag{7}$$

First, we select a discrete set $q \in \{1, \ldots, N\}$ of points along the x direction inside the grating period. Second, we define a set of N test functions which include the pseudoperiodicity factor as well:

$$T_q^N(x) = e^{-ik\alpha_0 x}\tilde{T}_q^N(x).$$

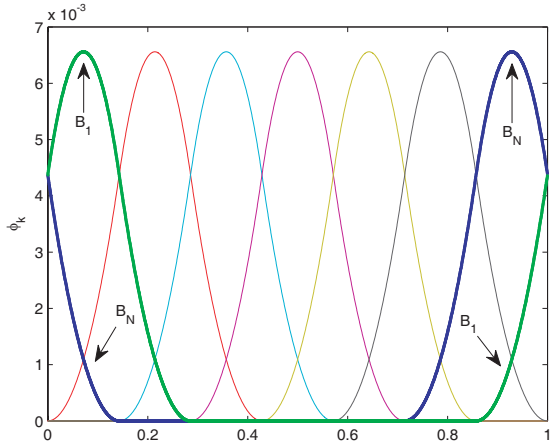

Figure 2. Sampling using a spline basis. The first and the last spline function are plotted in bold line to better illustrate the periodicity (normal incidence).

We use three different test functions: Dirac delta, pulse and spline. In the case of Dirac functions, the $\tilde{T}_q^N$ is:

$$\tilde{T}_q^N(x) = \delta\left(x - \left(q - \frac{1}{2}\right)\frac{d}{N}\right).$$

In the case of pulses, $\tilde{T}_q^N$ has the form below:

$$\tilde{T}_q^N(x) = \begin{cases} 1 & x \in \dfrac{d}{N}[q, q+1] \\ 0 & \text{otherwise.} \end{cases} \tag{8}$$

The third type of test function we employ is the second order spline B_n^N which is thus used as basis as well as test functions. This is a particular case of the Method of Moments known as the Galerkin Method.

In what follows we will denote by SDMM the Spline Dirac Modal Method, by SPMM the Spline Pulse Modal Method and by SSMM the Spline Spline Modal Method.

2.3. Matrix Eigenvalue Equation

Eliminating H_x and H_y in Equation (5) and E_x, E_y in Equation (6), we obtain an eigenvalue equation of the form:

$$\mathbf{L}F = r^2 F \tag{9}$$

where the eigenvector F is a column vector whose elements are the components E_{z_n} or H_{z_n} with the matrix operator $\mathbf{L}_{TE}$ and $\mathbf{L}_{TM}$ respectively:

$$\mathbf{L}_{TE} = \left[\mathbf{G}^{-1}\left(\frac{1}{k^2}\mathbf{D}\mathbf{G}^{-1}\mathbf{D} + \mathbf{G}^{\varepsilon}\right)\right] \tag{10a}$$

$$\mathbf{L}_{TM} = \left[\left(\mathbf{G}^{\frac{1}{\varepsilon}}\right)^{-1}\left(\frac{1}{k^2}\mathbf{D}\left(\mathbf{G}^{\varepsilon}\right)^{-1}\mathbf{D} + \mathbf{G}\right)\right] \tag{10b}$$

We denote $\mathbf{G}$, $\mathbf{D}$, $\mathbf{G}^{\varepsilon}$ and $\mathbf{G}^{\frac{1}{\varepsilon}}$ the square matrices expressing the inner products:

$$\mathbf{G} = \begin{pmatrix} \langle T_1^N, B_1^N\rangle & \cdots & \langle T_1^N, B_N^N\rangle \\ \vdots & \ddots & \vdots \\ \langle T_N^N, B_1^N\rangle & \cdots & \langle T_N^N, B_N^N\rangle \end{pmatrix}, \tag{11}$$

$$\mathbf{D} = \mathbf{D_0} - k^2\alpha_0^2\mathbf{G} \tag{12}$$

with

$$\mathbf{D_0} = \begin{pmatrix} \left\langle \tilde{T}_1^N, \frac{d}{dx}\tilde{B}_1^N \right\rangle & \cdots & \left\langle \tilde{T}_1, \frac{d}{dx}\tilde{B}_N^N \right\rangle \\ \vdots & \ddots & \vdots \\ \left\langle \tilde{T}_N, \frac{d}{dx}\tilde{B}_1^N \right\rangle & \cdots & \left\langle \tilde{T}_N, \frac{d}{dx}\tilde{B}_N^N \right\rangle \end{pmatrix}, \tag{13}$$

$$\mathbf{G}^{\varepsilon} = \begin{pmatrix} \left\langle T_1^N, \varepsilon B_1^N \right\rangle & \cdots & \left\langle T_1^N, \varepsilon B_N^N \right\rangle \\ \vdots & \ddots & \vdots \\ \left\langle T_N^N, \varepsilon B_1^N \right\rangle & \cdots & \left\langle T_N^N, \varepsilon B_N^N \right\rangle \end{pmatrix}, \tag{14}$$

$$\mathbf{G}^{\frac{1}{\varepsilon}} = \begin{pmatrix} \left\langle T_1^N, \frac{1}{\varepsilon} B_1^N \right\rangle & \cdots & \left\langle T_1^N, \frac{1}{\varepsilon} B_N^N \right\rangle \\ \vdots & \ddots & \vdots \\ \left\langle T_N^N, \frac{1}{\varepsilon} B_1^N \right\rangle & \cdots & \left\langle T_N^N, \frac{1}{\varepsilon} B_N^N \right\rangle \end{pmatrix}. \tag{15}$$

Where

$$\left\langle T_q^N, \varepsilon B_n^N \right\rangle = \int_0^d T_q^N(x)\, \varepsilon(x)\, B_n^N(x)\, dx \quad \text{and}$$

$$\left\langle T_q^N, \frac{1}{\varepsilon} B_n^N \right\rangle = \int_0^d T_q^N(x), \frac{1}{\varepsilon(x)} B_n^N(x)\, dx.$$

The calculation of the coefficients of matrix $\mathbf{G}$, $\mathbf{D}$, $\mathbf{G}^{\varepsilon}$ and $\mathbf{G}^{\frac{1}{\varepsilon}}$ from the Equations (10a) and (10b) include an inner product of the form $\left\langle T_q^N, B_n^N \right\rangle$ therefore an integral must be computed. Even though the integration limits range from 0 to d, the interval of actual integration is much smaller because of the compact support of the test and basis functions. By taking advantage of this property many entries can be directly identified to zero. An integral has to be computed only for those inner products in which the test and the basis functions overlap.

When dealing with the SDMM and SPMM each spline overlaps three test functions, therefore the matrix representing an inner product is tridiagonal. In the case of the SSMM however, each spline overlap five test functions and we get symmetrical sparse matrices with five diagonals. This is due to the fact that the length of the support for each basis and test function is $3d/N$. Each spline function $\tilde{B}_n^N$ overlaps two neighbors on its left ($\tilde{B}_{n-1}^N$ and $\tilde{B}_{n-2}^N$) two on its right ($\tilde{B}_{n+1}^N$ and $\tilde{B}_{n+2}^N$). We can also observe that a $\tilde{B}_n^N$ spline is nothing else but the translation to the right in the direction of the x axis by nd/N of the $\tilde{B}_0^N$, therefore all the inner products of the type $\langle B_n^N, B_n^N \rangle$ will have the same value. This holds true for the $\langle B_{n-1}^N, B_n^N \rangle$ and $\langle B_{n-2}^N, B_n^N \rangle$ as

well. All matrices having the same form, we detail only the **G** matrix of the SSMM:

$$\mathbf{G} = \begin{pmatrix} g_{11} & g_{12} & g_{13} & 0 & \cdots & 0 & g_{13} & g_{12} \\ g_{12} & g_{11} & g_{12} & g_{13} & 0 & \cdots & 0 & g_{13} \\ g_{13} & g_{12} & g_{11} & g_{12} & g_{13} & 0 & \cdots & 0 \\ & \ddots & \ddots & \ddots & \ddots & \ddots & & \\ & & \ddots & \ddots & \ddots & \ddots & \ddots & \\ 0 & \cdots & 0 & g_{13} & g_{12} & g_{11} & g_{12} & g_{13} \\ g_{13} & 0 & \cdots & 0 & g_{13} & g_{12} & g_{11} & g_{12} \\ g_{12} & g_{13} & 0 & \cdots & 0 & g_{13} & g_{12} & g_{11} \end{pmatrix} \tag{16}$$

In the case of the SDMM and SPMM each test function overlaps three basis functions so we only get tridiagonal matrices as already mentioned.

2.4. Boundary Conditions

The final step of the method consists in matching the continuous components of the fields at each interface between the regions. This allows us to determine the amplitude of the reflected and transmitted waves and to calculate the diffraction efficiencies.

The electric and magnetic component of the field E_z or H_z are computed as a finite expansion of eigenfunctions:

$$\Phi(x,y) = \sum_{m=1}^{N} (a_m e^{ikr_m y} + b_m e^{-ikr_m y}) F_m(x) \tag{17}$$

where

$$F_m(x) = \sum_{n=1}^{N} F_{nm} B_n^N(x)$$

The eigenvalues r_m are obtained from their square. If r_m^2 is real and positive, the regular square root is retained, whereas for a complex value of r_m^2, r_m is the square root with positive imaginary part. Hence, the waves with constant coefficient a_m and b_m correspond to forward and backward waves respectively. In order to write the boundary conditions we need to calculate the remaining tangential component of the electromagnetic field (E_x and H_x in TM and TE polarizations respectively). They are deduced from Equations (5) and (6) and computed as a finite expansion derived from the eigenfunction series by:

$$\Psi(x,y) = \sum_{n=1}^{N} \sum_{m=1}^{N} (a_m e^{ikr_m y} + b_m e^{-ikr_m y}) P_{nm} B_n^N(x) \tag{18}$$

Using Equations (5) and (6), the P_{nm}, in practice, are computed in their matrix form as:

$$[P_{nm}] = \begin{cases} \dfrac{k}{\omega\mu_0}[F_{nm}]\,[r_m] \text{ for TE polarization} \\ \dfrac{k}{\omega\varepsilon_0}\mathbf{G}^{-1}\mathbf{G}^{\frac{1}{\varepsilon}}[F_{nm}]\,[r_m] \text{ for TM polarization} \end{cases} \tag{19}$$

where $[r_m]$ is the diagonal matrix formed by the r_m. Boundary conditions are written using a $\mathbf{S}$ matrix formalism. The scattering matrices are obtained by projecting the continuous components of the fields onto the test functions.

Since we chose to use the same basis in every region it follows that the coefficients of the scattering matrices do not depend on the test functions, they only depend on the components of the eigenvectors.

2.5. Non Uniform Sampling Scheme

In order to improve the numerical results we use a non uniform sampling scheme. A change of variable $x = x(u)$ is defined so that a given variation Δu of u should result in a very much slower variation Δx of x in the neighborhood of $x = 0$, $x = fd$ and $x = d$ where the permittivity is discontinuous. A possible change of variable is the following:

$$x\,(u) = \begin{cases} u - \eta\dfrac{f}{2\pi}\sin\left(\dfrac{2\pi u}{fd}\right) & \text{for} \quad 0 \le u < fd \\ u + \eta\dfrac{1-f}{2\pi}\sin\left(\dfrac{2\pi\,(d-u)}{(1-f)\,d}\right) & \text{for} \quad fd \le u \le d \end{cases} \tag{20}$$

where η is a contraction parameter chosen between 0 and 1. When $\eta = 0$ there is no non uniform sampling and we find the previous case again. With this representation, the closer η is to 1, the higher the density of the points in the neighborhood of the discontinuity. We will show in the next section that the best result are obtained when η is set as close to 1 as possible. Figure 3 illustrates how the function $x(u)$ transforms an uniform discretization scheme into a non uniform one.

Introducing the adaptive sampling in Equations (10a) and (10b) gives us the operator form as:

$$\text{TE} : \left[\mathbf{G}^{-1}\left(\frac{1}{k^2}\mathbf{X}^{-1}\mathbf{D}\mathbf{G}^{-1}\mathbf{X}^{-1}\mathbf{D} + \mathbf{G}^{\varepsilon}\right)\right] \tag{21a}$$

$$\text{TM} : \left[\left(\mathbf{G}^{\frac{1}{\varepsilon}}\right)^{-1}\left(\frac{1}{k^2}\mathbf{X}^{-1}\mathbf{D}\,(\mathbf{G}^{\varepsilon})^{-1}\,\mathbf{X}^{-1}\mathbf{D} + \mathbf{G}\right)\right] \tag{21b}$$

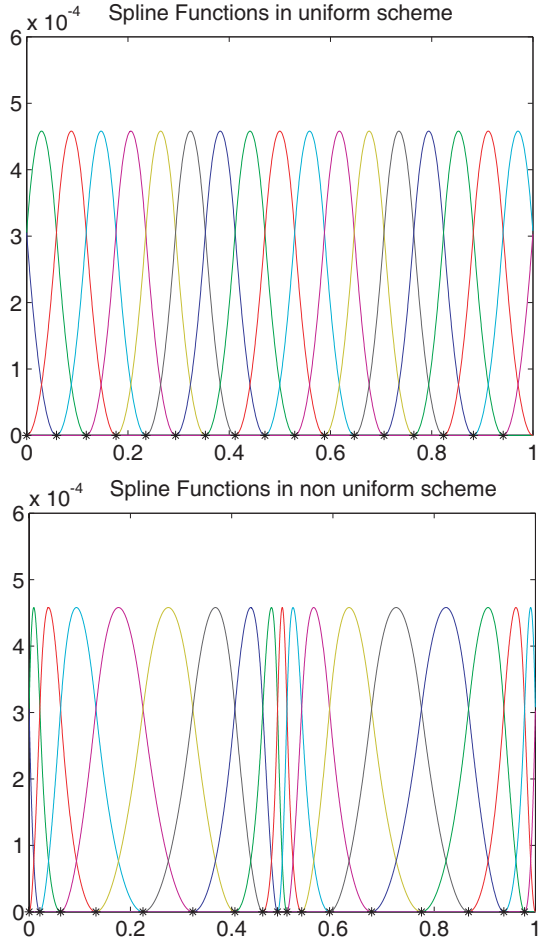

Figure 3. Illustration of the non uniform sampling scheme. The black stars are the discretization points. The contraction parameter is $\eta = 0$ in the upper figure (uniform sampling) and is set to $\eta = 0.75$ in the lower figure (non uniform sampling).

where $\mathbf{X}$ is the matrix form of the derivative of $x(u)$ given by $\mathbf{X} = \text{diag}\left(\frac{dx}{du}\right)$ evaluated at each discretization point x_n. This matrix takes into account the non uniform sampling.

It can be noticed that Equation (21b) is very similar to Equation (2) of Ref. [15].

3. NUMERICAL RESULTS

In the current section we provide numerical examples to illustrate the convergence speed of our method. Firstly, we show the improvement of the adaptive sampling scheme versus the uniform sampling scheme. Secondly, we compare our methods on typical cases of dielectric and metallic gratings in order to test their robustness and efficient implementation.

We systematically compare the convergence speed of the three methods described in detail in the previous sections, namely SDMM (Spline Dirac Modal Method), SPMM (Spline Pulse Modal Method) and SSMM (Spline Spline Modal Method). The enhanced Finite Difference Modal Method published by Lalanne and et al. [6] is used as a reference.

3.1. Non Uniform Versus Uniform Sampling Scheme

The following numerical results show the improvement of the adaptive sampling scheme. We choose a simple case of a dielectric lamellar grating with the following parameters: $\theta = 20°$, $d = 1\,\mu\text{m}$, $\lambda = 1\,\mu\text{m}$, $f = 0.5$, $\varepsilon_1 = 1$, $\varepsilon_{21} = 1$, $\varepsilon_{22} = 2.25$, $\varepsilon_3 = 2.25$.

We compare the specular diffraction efficiency using the uniform ($\eta = 0$) and the adaptive sampling scheme ($\eta = 0.5$ and $\eta = 0.9999$). Tables 1 and 2 list the numerical values calculated for each polarization. Using the parametric form presented in Section 2.5 the closer η to

Table 1. Diffraction efficiency of the zeroth order in TE polarization for different values of the contraction parameter.

N	$\eta = 0$	$\eta = 0.5$	$\eta = 0.9999$
7	0.02829269888588	0.02830453320569	0.02612252319351
9	0.02894069509428	0.02641523911226	0.02421909255991
11	0.02907295980140	0.02963321682395	0.02897873412815
13	0.02936157970815	0.02970434662757	0.02794674965262
21	0.02963401275171	0.02972449411195	0.02967315138327
31	0.02969689564078	0.02972163574224	0.02967464747408
41	0.02972409424861	0.02971840840399	0.02967437057689
51	0.02972236862175	0.02971167473470	0.02967413672271
61	0.02972473577342	0.02970803198096	0.02967396985251
71	0.02971970245739	0.02970368422456	0.02967384750402
81	0.02971872750592	0.02970112637523	0.02967375491827

Table 2. Diffraction efficiency of the zeroth order in TM polarization for different values of the contraction parameter.

N	$\eta = 0$	$\eta = 0.5$	$\eta = 0.9999$
7	0.31848428192847	0.26025017578805	0.06011645154005
9	0.02797285110395	0.01473159847140	0.01632844399267
11	0.00418537527986	0.01021265541234	0.01231436094980
13	0.01625621004825	0.00831770055047	0.01301618805031
21	0.01352659520124	0.01176570566895	0.01258501483037
31	0.01146468484695	0.01248186242394	0.01256453303296
41	0.01168869334432	0.01241874258224	0.01256088941295
51	0.01216942040848	0.01240736341067	0.01255926660915
61	0.01226329536845	0.01245891350365	0.01255862032993
71	0.01125041363728	0.01248035942563	0.01255829117276
81	0.01236790968004	0.01238333460826	0.01255812872220

1, the higher the density of the points in the neighborhood of the discontinuity. We observe that this yields to better numerical accuracy. On the other hand the adaptive method performance is similar to the uniform one for low truncation number (smaller than 20), but an outstanding improvement is obtained for larger truncation numbers. We get a precision of six digits whilst for the uniform scheme the precision is around three digits only. In the case of $\eta = 0.5$, the discretization points are not at the densest around the discontinuities. It correlates with a lower accuracy compared to the case where the contraction parameter is larger ($\eta = 0.9999$). Since our adaptive methods perform always better when we choose the parameter η very close to 1, we set this parameter $\eta = 0.9999$ for the upcoming examples.

3.2. Metallic Gratings

Our first test case is the metallic grating already analyzed in several research papers [6, 16]. The lamellar grating normalized pitch d/λ is set to 1, the normalized line width f is 0.5 and the normalized line height h/λ is 1. The metal permittivity is $\varepsilon_{22} = \varepsilon_3 = (0.22 - 6.71i)^2$. The angle of incidence θ is equal to 30°.

For this case, the reference eigenvalue with the smallest imaginary part, obtained from the exact modal method [1] is:

$$r = 0.40565997728692 - 0.00570953767335i \quad \text{for TE polarization}$$

$$r = 1.05070585861225 - 0.00180066465604i \quad \text{for TM polarization}$$

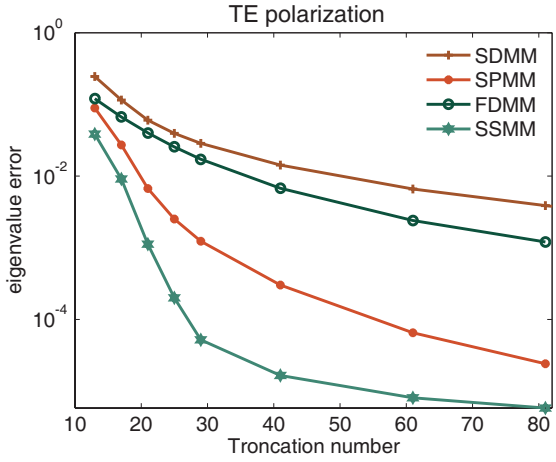

Figure 4. Relative error of the eigenvalue with the largest real part versus the truncation number in TE polarization for a metallic grating structure: $d/\lambda = 1$, $h/\lambda = 1$, $f = 0.5$, $\varepsilon_1 = \varepsilon_{21} = 1$ and $\varepsilon_{22} = \varepsilon_3 = (0.22 - 6.71i)^2$.

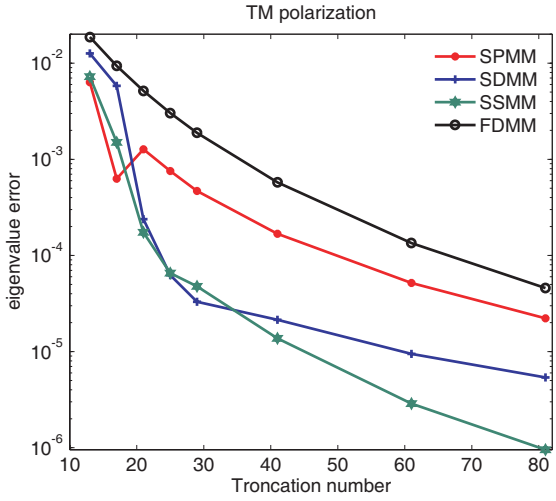

Figure 5. Relative error of the eigenvalue with the largest real part versus the truncation number in TM polarization for a metallic grating structure: $d/\lambda = 1$, $h/\lambda = 1$, $f = 0.5$, $\varepsilon_1 = \varepsilon_{21} = 1$ and $\varepsilon_{22} = \varepsilon_3 = (0.22 - 6.71i)^2$.

We define the relative error function as: $err_r(N) = |\frac{r^{(N)} - r}{r}|$ where $r^{(N)}$ is the computed eigenvalue with N basis retained in the calculation. In Figures 4 and 5, we plot this error in logarithmic scale for the TE and TM polarization respectively. The curve plotted with the circular markers denotes the FDMM results, the pluses are for SDMM, the dots are for SPMM and the stars for SSMM. This convention is used throughout the paper.

In Figure 4, a three-digit accuracy of the FDMM is reached when using a large number of basis functions (i.e., $N = 80$) whereas for the SPMM and SSMM this accuracy is obtained using a much smaller number of basis functions ($N = 20$, $N = 30$ respectively). A similar behavior can be observed in the TM polarization case (see Figure 5). The SDMM and SPMM implementation perform slightly better than the FDMM. The error of the SSMM decreases even more rapidly and we reach a four digit accuracy after a truncation numbers of $N = 30$.

In Figures 6 and 7 the relative errors of the minus-one diffraction order reflected efficiencies are plotted in logarithmic scale. The values of reference R_{ref} are taken from Table 1 of the Granet's adaptive implementation [16] using 201 basis functions. Up to the first five significant digits, the considered exact values are 0.73428 and 0.84848 for the TE and TM polarization respectively. In Figure 6, we can notice that the SSMM and SPMM perform better than FDMM, whilst

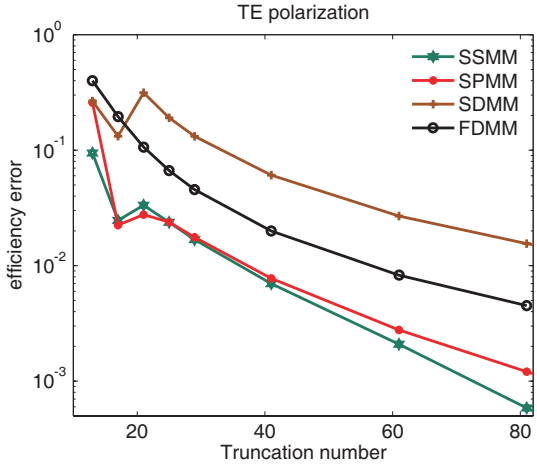

Figure 6. Relative error of the convergence of the -1 diffraction order efficiency for TE polarization for a metallic grating structure: $d/\lambda = 1$, $h/\lambda = 1$, $f = 0.5$, $\varepsilon_1 = \varepsilon_{21} = 1$ and $\varepsilon_{22} = \varepsilon_3 = (0.22 - 6.71i)^2$.

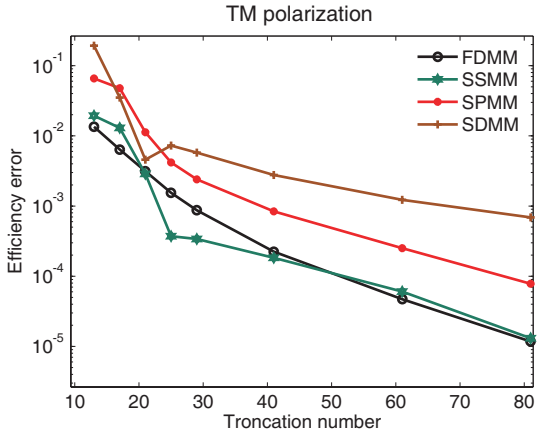

Figure 7. Relative error of the convergence of the -1 diffraction order efficiency for TM polarization for a metallic grating structure: $d/\lambda = 1$, $h/\lambda = 1$, $f = 0.5$, $\varepsilon_1 = \varepsilon_{21} = 1$ and $\varepsilon_{22} = \varepsilon_3 = (0.22 - 6.71i)^2$.

the SDMM performs not as well as the FDMM. In TM polarization (see Figure 7) the SSMM implementation provides a very good approximation even for the small truncation numbers. For the larger truncation numbers SSMM remain close to FDMM. In this case, the SPMM and SDMM performance is inferior to the FDMM.

To conclude, for the metallic gratings structures, it can be seen that our method based on spline expansion converges remarkably fast and the results remain stable even for unnecessary large truncation orders.

3.3. Dielectric Gratings

For our final example we take the case of a dielectric grating with a very large contrast between the refractive indices of the two transparent media from the grating zone. This test case has already been used in Ref. [16]. The incidence and geometrical parameters are: $\theta = 29°$, $\varepsilon_{21} = 1$, $\varepsilon_{22} = 25$, $d/\lambda = 1$, $f = 0.4$. For this case we look at the behavior of the second real eigenvalue when the real eigenvalues are sorted in ascending order. The exact values found using the exact modal method are: $r = 3.35101975722312$ and $r = 2.81329903403930$ for the TE and TM polarization respectively.

The convergence is illustrated in Figure 8 for the TE polarization and in Figure 9 for the TM polarization. The figures show the relative error plotted in logarithmic scale as a function of the truncation

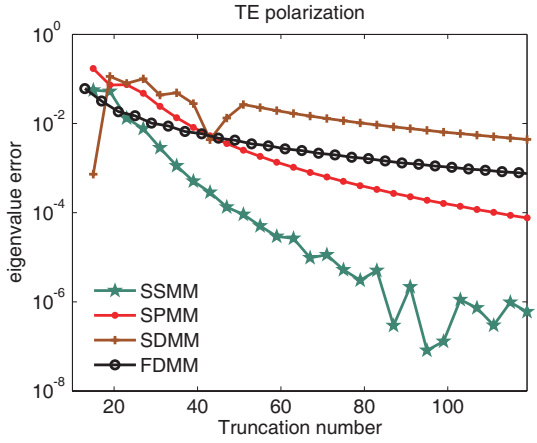

Figure 8. Relative error of the second smallest eigenvalue versus the truncation number in TE polarization: $\theta = 29°$, $\varepsilon_1 = \varepsilon_{21} = 1$, $\varepsilon_{22} = \varepsilon_3 = 25$, $d/\lambda = 1$, $h/\lambda = 1$ and $f = 0.4$.

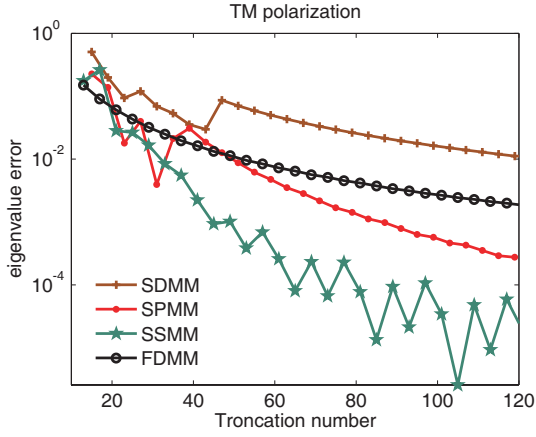

Figure 9. Relative error of the second smallest eigenvalue versus the truncation number in TM polarization: $\theta = 29°$, $\varepsilon_1 = \varepsilon_{21} = 1$, $\varepsilon_{22} = \varepsilon_3 = 25$, $d/\lambda = 1$, $h/\lambda = 1$ and $f = 0.4$.

number. Compared to the SPMM, the FDMM provides a better approximation only for the small truncation orders. But the overall convergence speed of the latter is significantly lower. We can see the huge improvement of the SSMM method versus all other implementations. We can also observe the oscillatory behavior of this

method. This is due to the fact that the sampling of the permittivity step can vary slightly depending on the truncation number. We did not put any other additional constraint to the sampling points.

3.4. Discussion of the Results

In every test case, our method shows a significantly improved convergence compared to FDMM. In addition, it has several interesting advantages. With FDMM we have a constraint for the discretisation points at the boundaries of the gratings: the mesh points have to be located on the permittivity discontinuities, whilst with our method they do not. The splines allow calculating the inner product analytically which improves the computation speed. Furthermore, this method offers symmetrical sparse matrices. Another strong point is that, in the way we implemented the adaptative sampling, we know that the optimal results are obtained when η is as close as possible to 1. For this reason the parameter was set to 0.9999. This is a major advantage compared to other methods that use an adaptive sampling scheme and need an optimization process in order to determine the best contraction parameter. We want also to point out the fact that our method can be applied to non-periodical problems almost without any modification. This can be a key point for the simulation examples of practical interest.

The SDMM is very sensitive to the choice of the sampling points. The results obtained are different when we change the point of interest. After several implementations we concluded that better performance is obtained when each Dirac point intersects three spline functions. Using the SPMM, we average on the region of interest, so this approach is less sensitive to the choice of the discretisation points. In the case of SSMM we get even less sensitive results. This is thanks to the fact that the test function is more elaborate, has a larger support and is therefore even less sensitive to the discretisation points. Furthermore the Galerkin method is reputed, from mathematical point of view, to provide more accurate results.

Our three implementations use the same basis function, the difference between them is the choice of test functions. Analyzing the error of the reflected efficiencies of these three implementations, we can see that, generally, we obtain more accurate results if the test functions are more elaborate.

4. CONCLUSION

In this paper, we numerically solve Maxwell's equations using a modal method based on spline expansion. The solution of the eigenvalue problem is obtained by using the method of moments: the unknown functions are expanded into a set of basis functions and the equations are projected onto a set of test functions. This approach was also used in the Finite Difference Modal Method. The fundamental difference between the latter and our approach is the choice of the basis and test functions.

In our method, the splines are chosen as basis functions and three test functions are used: the Dirac (point matching method), pulse and spline (Galerkin method) functions. We compare our implementations with other subsectional basis such as the pulse function (FDMM).

It is observed that a good accuracy is obtained even for small truncation numbers. The Spline Spline Modal Method performs especially well; it outperforms by far the reference method. Using the splines as basis functions is a promising start towards the introduction of hierarchical basis of spline wavelets functions. The implementation of a multiresolution analysis, preferably located around a region of the field with rapid variation is expected to provide an improved convergence, especially for the more isolated features. This new implementation will be illustrated in a future paper.

REFERENCES

1. Botten, L. C., M. C. Craig, R. C. McPherdran, L. R. Adams, and J. R. Andrewartha, "The dielectric lamellar diffraction grating," *Opt. Acta*, Vol. 28, 413–428, 1981.
2. Botten, L. C., M. C. Craig, R. C McPherdran, L. R. Adams, and J. R. Andrewartha, "The finitely conducting lamellar diffraction grating," *Opt. Acta*, Vol. 28, 1087–1102, 1981.
3. Moharam, M. G. and T. K. Gaylord, "Diffraction analysis of dielectric surface-relief gratings," *J. Opt. Soc. Am. A*, Vol. 72, 1385–1392, 1982.
4. Nevière, M. and E. Popov, *Light Propagation in Periodic Media: Differential Theory and Design*, Marcel Dekker, New York, 2003.
5. Morf, R. H., "Exponentially convergent and numerically efficient solution of Maxwell's equations for lamellar gratings," *J. Opt. Soc. Am.*, Vol. 12, No. 5, 1043–1056, 1995.
6. Lalanne, P. and J. P. Hugonin, "Numerical performance of finite-difference Modal Method for the electromagnetic analysis of one-

dimensional grating," *J. Opt. Soc. Am.*, Vol. 17, No. 6, 1033–1042, 2000.

7. Modisette, J. P., P. Nordlander, J. L. Kinsey, and B. R. Johnson, "Wavelet based in eigenvalue problems in quantum mechanics," *Chem. Phys. Letters*, Vol. 250, 485–428, 1996.
8. Beylkin, G., R. R. Coifman, and V. Rokhlin, "Fast wavelets transform and numerical algoritms I," *Comm. Pure and Appl. Math.*, Vol. 44, 141–183, 1991. Yale University Technical Report YALEU/DCS/RR-696, August 1989.
9. Wagner, R. L. and W. C. Chew, "A study of wavelets for the solution of electromagnetic intergal equations," *IEEE Trans. Antennas Propagat.*, Vol. 43, 614–622, June 1995.
10. Edee, K., P. Schiavone, and G. Granet, "Analysis of defect in extreme UV Lithography mask using a modal method based on nodal B-spline expansion," *Japanese Journal of Applied Physics*, Vol. 44, No. 9A, 6458–6462, 2005.
11. Armeanu, A., K. Edee, P. Schiavone, and G. Granet, "The lamellar diffraction grating problem: A spectral method based on spline expansion," *Proceedings of ICMI 2 Conference*, Vol. 19, No. 2, 37–46, 2009.
12. Jackson, J. D., *Classical Electrodynamics*, John Wiley and Sons, Inc., New York, 1962.
13. Harrington, R., *Field computation by Moment Methods*, The Macmillan, New York, 1968.
14. Harrington, R., "Matrix methods for field problem," *Proceeding of the IEEE*, Vol. 55. No. 2, 136–149, February 1967.
15. Guizal, B., H. Yala, and D. Felbacq, "Reformulation of the eigenvalue problem in the Fourier modal method with spatial adaptive resolution," *Opt. Lett.*, Vol. 34, No. 18, 2790–2792, 2009.
16. Granet, G., "Reformulation of the lamellar grating problem through the concept of adaptive spatial resolution," *J. Opt. Soc. Am.*, Vol. 16, No. 10, 2510–2516, 1999.